

Latest results on inclusive W/Z production at CMS

H. Wollny for the CMS Collaboration*

CERN

E-mail: Heiner.Wollny@cern.ch

At the LHC, inclusive production of W and Z -bosons offer a window to perform stringent tests of theoretical predictions based on the Standard Model (SM) and probe its fundamental parameters. With the large samples of W and Z events collected with the CMS detector, many processes have been studied at an unprecedented precision. These measurements test the SM predictions up to next-to-next-to-leading order and provide valuable inputs to improve the theoretical framework used to model LHC physics. In addition they put constraints on the parton distribution functions of the proton. In the following we will concentrate on the measurement of the fiducial Drell-Yan (DY) to muons cross-section at the Z -boson mass peak, double differentially in transverse momentum ($P_T(Z)$) and rapidity ($Y(Z)$), as it was presented for the first time during this conference.

*XXII. International Workshop on Deep-Inelastic Scattering and Related Subjects,
28 April - 2 May 2014
Warsaw, Poland*

*Speaker.

1. Introduction

The production of W and Z production is a prominent hard scattering process at hadron colliders. Because of the large production cross-sections, both are important backgrounds for Higgs and beyond standard model searches. Now, with the high integrated luminosity collected at the LHC the W and Z production are measured with great precision and tests theoretical predictions which are available at next-to-next-to leading order (NNLO) in perturbative QCD. In addition, those measurements put constraints on the parton distribution functions (PDF) of the proton. At CMS several precision measurements were performed using the 7 TeV and the 8 TeV data sets collected in 2011 and 2012, respectively. In this proceeding we will concentrate on the measurement of the fiducial Drell-Yan (DY) to muons cross-section at the Z -boson mass peak, double differentially in transverse momentum ($P_T(Z)$) and rapidity ($Y(Z)$), as it is presented for the first time during this conference. The analysis is done using the full 8 TeV data set with an integrated luminosity of 19.7 fb^{-1} . The measurement tests the QCD dynamics via the Drell-Yan process in a large kinematic range. Furthermore, for higher $P_T(Z)$, where the production is dominated by gluon-quark scattering, it is sensitive to the gluon PDF. In particular, in a region relevant for the gluon fusion production of the Higgs-boson. This measurement complements the results of other processes, like direct photon production [1] and top pair production [2], which put constrain on the gluon PDF too. Differential Z production at the LHC has been previously studied in [3, 4, 5, 6, 7, 8, 9, 10, 11].

2. Experiment

The central feature of the Compact Muon Solenoid (CMS) [12] apparatus is a superconducting solenoid of 6 m internal diameter, providing a magnetic field of 3.8 T. Within the superconducting solenoid volume are a silicon pixel and strip tracker, a lead tungsten crystal electromagnetic calorimeter (ECAL), and a brass/scintillator hadron calorimeter (HCAL), each composed of a barrel and two end-cap sections. Muons are measured in gas-ionization detectors embedded in the steel flux-return yoke outside the solenoid. Extensive forward calorimetry complements the coverage provided by the barrel and end-cap detectors. Muons are measured in the pseudo-rapidity range $|\eta| < 2.4$, with detection planes made using three technologies: drift tubes, cathode strip chambers, and resistive plate chambers.

3. Event Selection

The analyzed event sample was recorded by an isolated single muon trigger. This trigger selects muons with transverse momenta ($p_T(\mu)$) greater than 24 GeV and absolute pseudo-rapidities ($|\eta|$) up to 2.1. The particle-flow event reconstruction [13, 14] is used in this analysis. It consists in reconstructing and identifying each single particle with an optimized combination of all sub-detector information. For the offline selection of the muons the standard CMS muon selection is used [15]. It requires that the muon candidate is reconstructed both in the muon chambers and the inner tracker devices and that the reduced χ^2 of the global fit is better than 10. In addition, a minimum number of hits in the pixel, inner tracker layers and in the muon chambers is requested. Also it is required that the distance between the muon candidate trajectory and the primary vertex

is smaller than 2 mm and 5 mm in the transverse plane and longitudinal direction, respectively. As primary vertex the one with the highest sum of squared transverse momenta of associated tracks is selected. In order to suppress background it is required that the muons are isolated. The isolation is based on particle flow candidates within a cone of 0.4 in $\Delta R = \sqrt{\Delta\eta^2 + \Delta\phi^2}$ and it is corrected for contributions from additional proton-proton interactions per event (pileup). Charged pileup contributions are identified by not coming from the primary vertex and neutral contributions from the pileup are estimated using a naive average of neutral to charged contributions (0.5), which was measured in jets. The relative isolation is required to be smaller 0.12 (0.5) for the leading (second) muon. The choice for the loosen up isolation of the second muon is motivated by the event kinematics, as the second muon often points into the region of the hadronic recoil balancing the transverse momentum of the Z-boson. Finally, the leading muon is required to be matched to the trigger and is selected in the kinematic range with $p_T(\mu) > 25 \text{ GeV}$ and $|\eta| < 2.1$. For the second muon no trigger matching is imposed and it is selected in the range with $p_T(\mu) > 10 \text{ GeV}$ and $|\eta| < 2.4$. The absolute rapidity, $|Y(Z)|$, of the opposite charged muon pair is selected below 2 and the invariant mass is selected between 81 and 101 GeV. In the rare case of ambiguity the muon pair with the invariant mass closest to the Z-boson mass is selected.

The events are binned in 10 bins in $P_T(Z)$ and five bins in $|Y(Z)|$. The bins in $P_T(Z)$ are [0,20], [20,40], [40,60], [60,80], [80,100], [100,120], [120,140], [140,170], [170,200], [200,∞] and in $|Y(Z)|$ they are [0,0.4], [0.4,0.8], [0.8,1.2], [1.2,1.6] and [1.6,2.0].

4. Analysis

The signal process is simulated using the MADGRAPH 1.3.30 [16] generator with 0 to 4 additional jets, interfaced with PYTHIA6 [17] with Z2star tune for hadronization and parton shower effects with a matching scale of 20 GeV. Multiple-parton-interaction is accounted for via PYTHIA6. QED initial state radiation is not included. The CTEQ6L1 [18] PDF was selected for the generation. The backgrounds were generated either with MADGRAPH (W+jets, $t\bar{t}$, $\tau\tau$), POWHEG [19] (single top [20, 21]), or PYTHIA6 [17] for di-bosons (WW, WZ, ZZ). The inclusive cross-sections of DY , W [22], and $t\bar{t}$ [23] are normalized to NNLO. Also for single top a higher order (approximate NNLO) inclusive cross-section was used. The generated events are passed through a detector simulation based on GEANT4 [24].

The cross-section measurement relies strongly on the simulation of the detector and on the knowledge of the backgrounds. In order to reduce the dependence on the simulation the efficiencies for the tracking, the trigger, the identification and the isolation of the muons are determined in a data-driven way using a tag and probe method [15]. The efficiencies are measured in simulation and data and the differences are accounted for by scale factors. The efficiencies are in general measured as a function of transverse momentum and pseudorapidity of the muons. For the trigger also the muon charge is considered. Great care was taken in measuring the isolation efficiency of the second muons as it is correlated with the event kinematics, i.e. the hadronic recoil of the Z-boson, as the second muons often go in this direction. For that reason the isolation of the second muon is chosen more loose than for the leading muon and the efficiency is measured three dimensional in $P_T(Z)$, $\cos\theta^*$ and $|\phi^*|$, where θ^* and ϕ^* are the polar and the azimuthal angles, respectively, measured in the helicity frame. Also the background yields for $t\bar{t}$, $DY \rightarrow \tau\tau$, WW, tW , $\bar{t}W$, and

W +jets are estimated in a data-driven way. These backgrounds have typically two prompt leptons in the final state where the flavor of the two can be arbitrary. The method is based on the following assumption: $\frac{N_{\mu\mu}^{MC}}{N_{e\mu}^{MC}} = \frac{N_{\mu\mu}^{Data}}{N_{e\mu}^{Data}}$, namely that the fraction of having two opposite signed muons ($\mu\mu$ -channel) or having one electron and one muon with opposite charge ($e\mu$ -channel) in the final state is the same for simulation and data. Hence, the ratio of the yields of data and simulation in the $e\mu$ -channel can be used to normalize the simulation in the $\mu\mu$ -channel. No significant trend in $P_T(Z)$ and $|Y(Z)|$ is observed for the scaling factor and hence a constant factor is used and a 10% uncertainty is assigned. The described method is not used to normalize the event yields of the WZ and the ZZ backgrounds. These backgrounds include a true $Z \rightarrow \mu\mu$ decay, and it is hence quite unlikely to select an opposite charged electron-muon pair instead. Here the yields are taken from simulation and a conservative uncertainty of 50% is assigned. The estimated backgrounds are small, at maximum 2%. They are subtracted from the data before the unfolding is performed. In order to avoid a bias in the response matrix and in the acceptance due to imprecise modeling of the Z -boson kinematics, the simulation is weighted in fine bins of $P_T(Z)$ and $Y(Z)$ to match the distributions of data. For the weights a variable binning in $P_T(Z)$ and $Y(Z)$ is used to ensure sufficient amount of data in each bin. As the weights are determined on reconstruction level but applied on generator level the weighting procedure is repeated until the change of the results with respect to the previous iteration is small. It was verified that with each iteration the difference is getting smaller. The procedure was stopped after seven iterations. For the main part of the bins the change is below 1 per mille already after the first iteration.

Finally, the reconstructed and background-corrected double-differential $P_T(Z)$ and $|Y(Z)|$ distribution is unfolded to the pre-final state radiation distribution. In order to reduce the dependence on the simulation the unfolding is performed to the fiducial region within the acceptance of the leading and the second muon, within the mass range $81 \leq M(\mu\mu) < 101$ GeV, and within the rapidity region $|Y(Z)| < 2$. For the unfolding the ‘iterative Bayesian’ method [25] implemented in the RooUnfold package [26] is used.

The systematic uncertainties of the measurement are carefully studied. The dominant ones are the uncertainties on the luminosity and on the efficiency correction factors. Already one order of magnitude smaller are the systematic uncertainties from pileup and final state radiation. The systematic uncertainties from the background subtraction, the unfolding, the muon momentum resolution and scale are another order of magnitude smaller.

5. Results

In Fig. 1 the double-differential cross-section measurement is compared to the MadGraph (red) and the RESBOS [27, 28, 29] (blue) generator. The RESBOS generation is in approximate NNLO and the CT10nnlo [30] PDF set was used. Shown is the $P_T(Z)$ dependence for the five bins in $|Y(Z)|$. For the comparison the leading order MadGraph cross-section was scaled to the next-to-next-to-leading order cross-section computed with FEWZ. In the bottom panels the corresponding ratio of simulation and data is shown. The open circles represent the ratio with MadGraph and the open triangles the ratio with RESBOS. The error bars represent the statistical uncertainties of data and simulation whereas the hatched bands represent the systematic uncertainties of the data only. For a better comparison of trends in $P_T(Z)$ and $|Y(Z)|$ the single differential cross-sections in

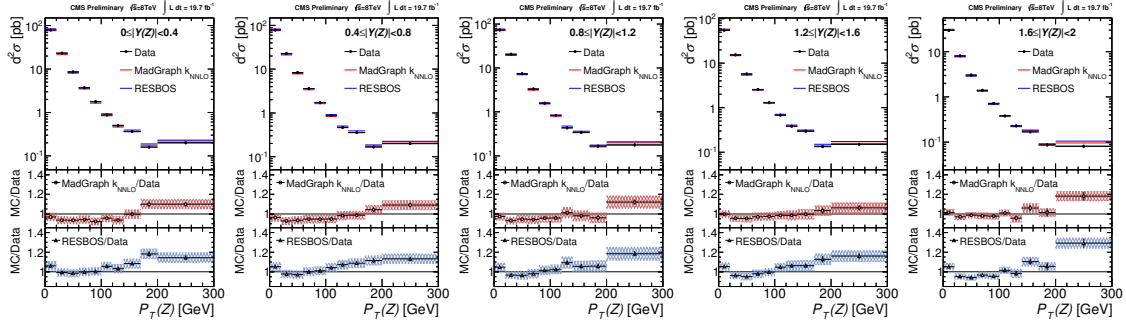


Figure 1: Comparison of the $P_T(Z)$ dependence in six bins of $|Y(Z)|$ of the fiducial cross-section with MADGRAPH generator normalized to NNLO (red) and RESBOS generator (blue).

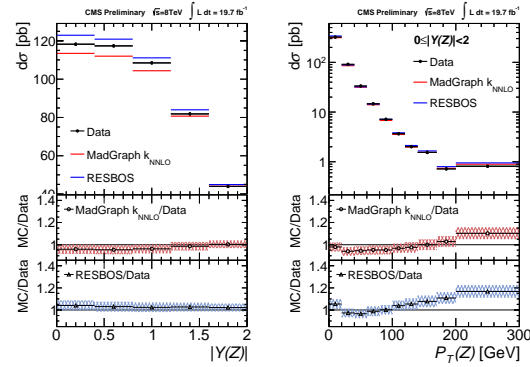


Figure 2: Comparison of the $|Y(Z)|$ and $P_T(Z)$ dependence of the fiducial cross-section with MADGRAPH generator normalized to NNLO (red) and RESBOS generator (blue).

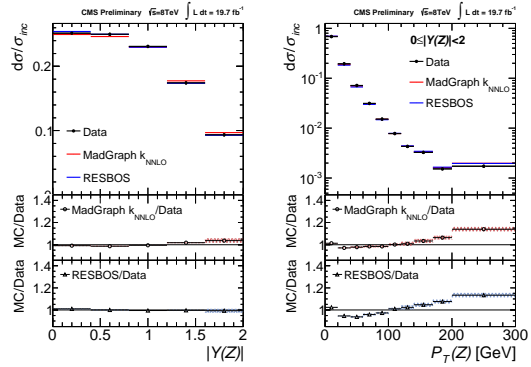


Figure 3: Comparison of the $|Y(Z)|$ and $P_T(Z)$ dependence of the normalized fiducial cross-section with MADGRAPH generator normalized to NNLO (red) and RESBOS generator (blue).

these variables are shown in Fig. 2. As can be seen on the left overshoots MadGraph data by about 5% and RESBOS undershoots data by about 5%. Both generators show a similar trend in $P_T(Z)$ compared to data. This is better visible for the normalized cross-section, where the measurement is divided by the inclusive cross-section. The comparison is shown in Fig. 3. Both generator describe reasonable the shape in rapidity but fails to reproduce the shape in $P_T(Z)$.

References

[1] D. d’Enterria and J. Rojo *Nucl.Phys.* **B860** (2012) 311–338, arXiv:1202.1762.
 [2] M. Czakon, M. L. Mangano, A. Mitov, and J. Rojo *JHEP* **1307** (2013) 167, arXiv:1303.7215.
 [3] CMS Collaboration, S. Chatrchyan *et al.* *Phys.Rev.* **D85** (2012) 032002, arXiv:1110.4973.
 [4] ATLAS Collaboration, G. Aad *et al.* arXiv:1406.3660.
 [5] ATLAS Collaboration, G. Aad *et al.* *Phys.Lett.* **B705** (2011) 415–434, arXiv:1107.2381.
 [6] CMS Collaboration. CMS-PAS-SMP-12-025.

- [7] **LHCb** Collaboration. LHCb-CONF-2013-007, CERN-LHCb-CONF-2013-007.
- [8] **LHCb** Collaboration, R. Aaij *et al.* *JHEP* **1302** (2013) 106, [arXiv:1212.4620](#).
- [9] **LHCb** Collaboration, R. Aaij *et al.* *JHEP* **1206** (2012) 058, [arXiv:1204.1620](#).
- [10] **CMS** Collaboration, S. Chatrchyan *et al.* *JHEP* **1312** (2013) 030, [arXiv:1310.7291](#).
- [11] **ATLAS** Collaboration, G. Aad *et al.* *Phys.Lett.* **B720** (2013) 32–51, [arXiv:1211.6899](#).
- [12] **CMS** Collaboration, S. Chatrchyan *et al.* *JINST* **3** (2008) S08004.
- [13] **CMS** Collaboration. CMS-PAS-PFT-09-001.
- [14] **CMS** Collaboration. CMS-PAS-PFT-10-001.
- [15] **CMS** Collaboration, S. Chatrchyan *et al.* *JINST* **7** (2012) P10002, [arXiv:1206.4071](#).
- [16] J. Alwall, M. Herquet, F. Maltoni, O. Mattelaer, and T. Stelzer *JHEP* **1106** (2011) 128, [arXiv:1106.0522](#).
- [17] T. Sjostrand, S. Mrenna, and P. Z. Skands *JHEP* **0605** (2006) 026, [arXiv:hep-ph/0603175](#).
- [18] P. Nadolsky, J. Gao, M. Guzzi, J. Huston, H.-L. Lai, *et al.* [arXiv:1206.3321](#).
- [19] S. Alioli, P. Nason, C. Oleari, and E. Re *JHEP* **1006** (2010) 043, [arXiv:1002.2581](#).
- [20] S. Alioli, P. Nason, C. Oleari, and E. Re *JHEP* **0909** (2009) 111, [arXiv:0907.4076](#).
- [21] E. Re *Eur.Phys.J.* **C71** (2011) 1547, [arXiv:1009.2450](#).
- [22] R. Gavin, Y. Li, F. Petriello, and S. Quackenbush *Comput.Phys.Commun.* **182** (2011) 2388–2403, [arXiv:1011.3540](#).
- [23] M. Czakon, P. Fiedler, and A. Mitov *Phys.Rev.Lett.* **110** (2013) no.~25, 252004, [arXiv:1303.6254](#).
- [24] **GEANT4** Collaboration, S. Agostinelli *et al.* *Nucl.Instrum.Meth.* **A506** (2003) 250–303.
- [25] G. D’Agostini *Nucl.Instrum.Meth.* **A362** (1995) 487–498.
- [26] T. Auye [arXiv:1105.1160](#).
- [27] G. Ladinsky and C. Yuan *Phys.Rev.* **D50** (1994) 4239, [arXiv:hep-ph/9311341](#).
- [28] F. Landry, R. Brock, P. M. Nadolsky, and C. Yuan *Phys.Rev.* **D67** (2003) 073016, [arXiv:hep-ph/0212159](#).
- [29] C. Balazs and C. Yuan *Phys.Rev.* **D56** (1997) 5558–5583, [arXiv:hep-ph/9704258](#).
- [30] J. Gao, M. Guzzi, J. Huston, H.-L. Lai, Z. Li, *et al.* *Phys.Rev.* **D89** (2014) 033009, [arXiv:1302.6246](#).